AGU PUBLICATIONS

JGR

Journal of Geophysical Research: Planets

RESEARCH ARTICLE
10.1002/2014JE004761

Limited role for thermal erosion by turbulent lava in proximal Athabasca Valles, Mars

Vincenzo Cataldo[1], David A. Williams[1], Colin M. Dundas[2], and Laszlo P. Keszthelyi[2]

[1]School of Earth and Space Exploration, Arizona State University, Tempe, Arizona, USA, [2]Astrogeology Science Center, U.S. Geological Survey, Flagstaff, Arizona, USA

Key Points:
- Thermal erosion by turbulent lava is investigated in proximal Athabasca, Mars
- Modeled erosion depths are far less than the depth of the Athabasca channel
- Thermal erosion alone does not appear to have formed the Athabasca channel

Correspondence to:
V. Cataldo,
Vincenzo.Cataldo@asu.edu

Citation:
Cataldo, V., D. A. Williams, C. M. Dundas, and L. P. Keszthelyi (2015), Limited role for thermal erosion by turbulent lava in proximal Athabasca Valles, Mars, *J. Geophys. Res. Planets*, *120*, 1800–1819, doi:10.1002/2014JE004761.

Received 14 NOV 2014
Accepted 13 OCT 2015
Accepted article online 22 OCT 2015
Published online 21 NOV 2015

Abstract The Athabasca Valles flood lava is among the most recent (<50 Ma) and best preserved effusive lava flows on Mars and was probably emplaced turbulently. The Williams et al. (2005) model of thermal erosion by lava has been applied to what we term "proximal Athabasca," the 75 km long upstream portion of Athabasca Valles. For emplacement volumes of 5000 and 7500 km^3 and average flow thicknesses of 20 and 30 m, the duration of the eruption varies between ~11 and ~37 days. The erosion of the lava flow substrate is investigated for three eruption temperatures (1270°C, 1260°C, and 1250°C), and volatile contents equivalent to 0–65 vol % bubbles. The largest erosion depths of ~3.8–7.5 m are at the lava source, for 20 m thick and bubble-free flows that erupted at their liquidus temperature (1270°C). A substrate containing 25 vol % ice leads to maximum erosion. A lava temperature 20°C below liquidus reduces erosion depths by a factor of ~2.2. If flow viscosity increases with increasing bubble content in the lava, the presence of 30–50 vol % bubbles leads to erosion depths lower than those relative to bubble-free lava by a factor of ~2.4. The presence of 25 vol % ice in the substrate increases erosion depths by a factor of 1.3. Nevertheless, modeled erosion depths, consistent with the emplacement volume and flow duration constraints, are far less than the depth of the channel (~35–100 m). We conclude that thermal erosion does not appear to have had a major role in excavating Athabasca Valles.

1. Introduction

1.1. Flood Lava at Athabasca Valles

Athabasca Valles is a 300 km long outflow channel located in north-central Elysium Planitia, Mars. It has a crater retention age of 20 Ma or less [e.g., *Berman and Hartmann*, 2002; *Burr et al*., 2002], but the channel may be older because those ages refer to the lava coating the channel [*McEwen et al*., 2012]. *Jaeger et al*. [2007, 2010] studied the few tens of meters thick lava flow that drapes the Athabasca channel system—among the best preserved and youngest flood lavas on Mars [*Plescia*, 1990]. The flow issued simultaneously from a series of vents located along a fissure that is part of the Cerberus Fossae and extended southwest for about 300 km through Athabasca Valles. It then emptied into a basin named Cerberus Palus and spread over the surrounding plains, flowing as far as ~1400 km from its source (see Figure 1). Crater retention ages in the range 0.5–10 Ma were derived, based on the observed superposition of secondary impact craters onto the flow [*Jaeger et al*., 2010, and references therein]. Thickness estimates that reflect the thickness of the solidified lava where it pooled on the Cerberus Palus plain are in the range 20–30 m and were obtained from the volume of the partially degassed lava which *Jaeger et al*. [2010] calculated to be in the range of 5000–7500 km^3. As a result, the volume of lava including bubbles that flowed out of the vent may have been somewhat higher. Flow thicknesses of 80–100 m were reached in the center of the channel at maximum flow rate. At its greatest thickness, the flow locally overtopped the channel banks. Subsequently, as fluid lava drained downstream into the distal basin of Cerberus Palus, the lava flow thickness dropped more than 50 m from its highstand [*Jaeger et al*., 2007]. The total width of the Athabasca channel system is ~30–50 km (with an average value of 39 km), and the average slope is 0.063 ± 0.007% (0.036° ± 0.004°) [*Jaeger et al*., 2010].

Instrumentation aboard the Mars Reconnaissance Orbiter (MRO) was used to investigate the morphology and composition of the flow to constrain its emplacement. Specifically, the 27–117 cm/pixel color and stereo High Resolution Imaging Science Experiment (HiRISE) [*McEwen et al*., 2007] images, together with the ~6 m/pixel context camera (CTX) [*Malin et al*., 2007] images enabled flow margins and contacts to be resolved.

Flood lavas are characterized by large volumes and areal coverage. Early quantitative studies of terrestrial flood basalts suggested that they were emplaced in a turbulent fashion [*Shaw and Swanson*, 1970], but

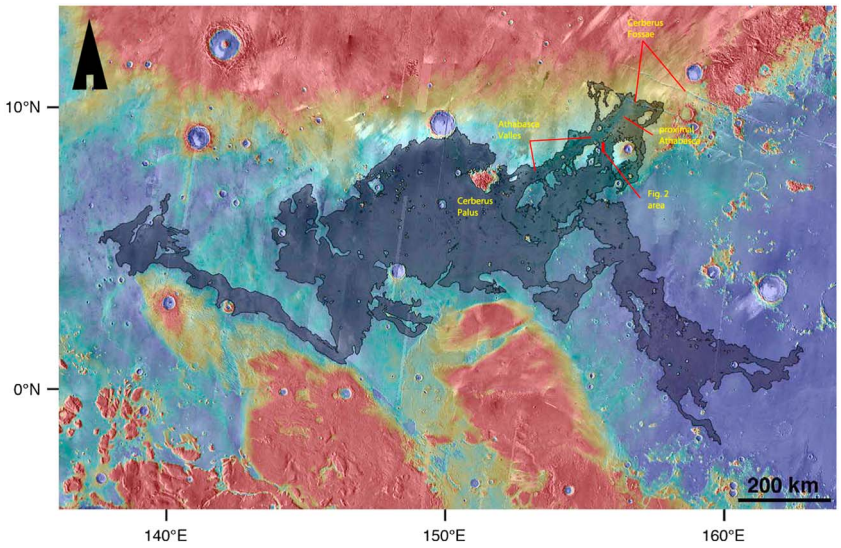

Figure 1. The Athabasca flood lava, as mapped from Mars Reconnaissance Orbiter (MRO) data, and colorized with MOLA gridded data [from *Jaeger et al.*, 2010]. The lava source region is Cerberus Fossae, the system of fissures located NE of the flow. The proximal Athabasca region extends 75 km in the southwest direction whereas Athabasca Valles stretches to a distance of ~300 km from the lava source. The orange box southwest of proximal Athabasca covers the area shown in Figure 2.

detailed examination of the lava flow morphologies suggested laminar emplacement under a thick insulating crust [*Self et al.*, 1998]. On Earth, the study of features diagnostic of inflation in flood lavas indicates emplacement in a laminar flow regime [*Hon et al.*, 1994] and long eruption durations [*Self et al.*, 1998]. The Athabasca Valles lava flow is a few meters thick within a distance of 75 km from its source (proximal Athabasca) and gradually thickens to a few tens of meters in the downstream direction. Thus, the flow apparently deflated rather than inflated in its proximal portions before solidifying [*Jaeger et al.*, 2010]. The same authors found that the lava flow was likely emplaced during a single event over a period of a few to several weeks and, at peak discharge, was partially to fully turbulent (with a Reynolds number, Re = 860–300,000; the transition to turbulence occurs around Re = 500–2000, *Bird et al.* [1960]). *Jaeger et al.* [2010] used reasonable physical properties for the lava and the observed dimensions of the channel to calculate flow velocity and lava volume flux [following *Keszthelyi et al.*, 2006] and, using these results, derived information about flow regime. Lava composition is difficult to determine because the lava flow region is currently overlain by sufficient dust to obscure substrate mineralogy [*Bandfield et al.*, 2000; *Christensen et al.*, 2001]. However, mineralogical maps produced from data collected utilizing the Compact Reconnaissance Imaging Spectrometer (CRISM), with a spatial resolution of 15–19 m/pixel [*Murchie et al.*, 2007], provided some insight into the composition of the Athabasca flood lava [*Jaeger et al.*, 2010]. CRISM data confirmed that the Athabasca flood lava is spectrally similar to the mafic-ultramafic materials seen by Spirit in Gusev crater [*Jaeger et al.*, 2010]—the so-called "Adirondack" type lavas—which show a composition intermediate to that of a basalt and a picrobasalt [*McSween et al.*, 2004, 2008] and are comparable with terrestrial high-Mg basalts or komatiitic basalts [*Gellert et al.*, 2004].

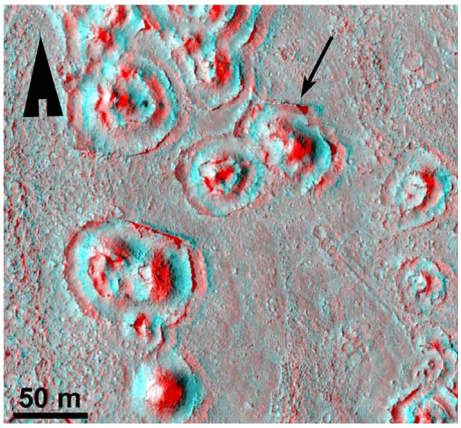

Figure 2. Subregion of an anaglyph produced from HiRISE stereo image pair PSP_001540_1890 and PSP_002371_1890. Coordinates of image center are 8°N, 156°E. The arrow points to a piece of solidified lava crust that was broken and upended in response to the loading of the lava surface by the growth of a hydrovolcanic (rootless) cone [from *Jaeger et al.*, 2010].

Thousands of ring-mound landforms [*Jaeger et al.*, 2007] occur exclusively on the Athabasca Valles lava flow surface, commonly near channel margins. HiRISE observations cast

light on these landforms, which are now thought to be hydrovolcanic or rootless cones, formed when ice and/or groundwater heated by the overlying lava flow vented in steam explosions (see Figure 2).

1.2. Thermal Erosion by Turbulently Flowing Lava at Athabasca

The partial or complete melting and assimilation of a solid or particulate substrate by flowing lava are defined as thermal erosion, whereas mechanical erosion involves the entrainment of substrate materials that have not chemically interacted with the lava [*Williams et al*., 1998]. Thermomechanical erosion implies a combination of the two processes. These processes are important because they cause the removal of substrate during lava flow emplacement, and erosion by flowing lava is a mechanism thought to be responsible for the formation of some lava channels and tubes on Earth and other silicate planets and moons [e.g., *Carr*, 1974; *Baker et al*., 1992; *Greeley et al*., 1998; *Schenk and Williams*, 2004; *Head et al*., 2011]. Regardless of the mechanism, erosion by lava is most plausible for high-temperature, low-viscosity lavas, especially if they flow turbulently. For Mars, erosion by lava has been considered a possible mechanism for the generation of at least some of the channels occurring in volcanic areas as an alternative to flowing water [e.g., *Carr*, 1974; *Baird*, 1984; *Cutts et al*., 1978; *Wilson and Mouginis-Mark*, 1984, 2001; *Leverington*, 2011; *Williams et al*., 2005; *Hurwitz et al*., 2010]. *Dundas and Keszthelyi* [2014] described evidence for local mechanical erosion by a turbulent flood lava flow in Kasei Valles on Mars, with kilometer-scale headwall retreat at several cataracts defined by tens to hundreds of meters of relief. Nevertheless, the same authors found that the flow was far from adequate to erode that large channel. Athabasca Valles and several other outflow channels with depths $\leq$100 m are found in the Elysium Planitia region. The scale of those channels, and evidence for extensive recent flood volcanism, makes it necessary to understand and quantify the potential for erosion by lava there.

Hulme [1973] simulated the role played by high-temperature, low-viscosity, and high-density lavas in creating the sinuous rilles on the Moon. *Hulme* [1973] and *Huppert and Sparks* [1985] showed that turbulently flowing, low-viscosity lavas are expected to lose heat mainly by convection rather than conduction. *Huppert et al*. [1984] and *Huppert and Sparks* [1985] used a combination of laboratory experiments and mathematical modeling to simulate the turbulent emplacement of Archean komatiites on Earth. In subsequent years, all workers used variations of the Hulme model and the Huppert and Sparks model [e.g., *Coombs et al*., 1988; *Jarvis*, 1995; *Williams-Jones et al*., 1998; *Wilson and Mouginis-Mark*, 2001].

The rigorous analytical-numerical model developed by *Williams et al*. [1998] advances the *Huppert and Sparks* [1985] model by involving both a geophysical approach and a geochemical approach, thus better constraining the composition and thermal-rheological properties of lava and substrate, and the convective heat transfer to the top of the flow and to the substrate. Furthermore, it was designed for terrestrial localities where model results could be compared to field data. The *Williams et al*. [1998, 2000a, 2000b, 2005] model has been used to investigate thermal erosion by turbulent lava under various conditions on Earth, the Moon, Io, and Mars and calculates erosion rates and depths with time, as a function of distance from the source.

Jaeger et al. [2010] suggested that the brief duration of the Athabasca Valles Flood Lava eruption implied little thermal erosion but did not quantify the plausible amount. Here we apply the *Williams et al*. [2000a, 2005] model to "proximal Athabasca," the upstream portion of Athabasca Valles, which stretches to a distance of ~75 km from the lava source. Our objective is to investigate if the Athabasca Valles lava may have flowed turbulently out to the maximum distance traveled and determine erosion rates and depths across the entire length of proximal Athabasca. We want to assess what role, if any, thermal erosion played in the formation of Athabasca Valles. We then compare model results with available observations.

2. Methodology

2.1. The Model

The model adopted is taken from *Williams et al*. [2005], and we report here the suite of the main equations that are assembled into a C-written code. The flow is one-dimensional with thermal erosion in the vertical direction. Lava erupts as a turbulent flow with a thermally mixed interior, convective heat transfer occurs to the top and the base of the flow, and thermal erosion occurs at the base of the flow, providing that the lava temperature is greater than the melting temperature of the substrate and latent heat is released as the flow crystallizes. The model includes (1) the effects of lava rheology changes due to assimilation of eroded substrate and crystallization of mafic minerals in the flowing lava, (2) the lava temperature decrease as the

AGU Journal of Geophysical Research: Planets

10.1002/2014JE004761

Table 1. Input Values for Modeling Low-Viscosity Lava Emplacement at Proximal Athabasca, Mars

	SiO_2	TiO_2	Al_2O_3	Fe_2O_3	FeO	MnO	MgO	CaO	Na_2O	K_2O	P_2O_5	
						wt%						
	45.4	0.46	10.9	3.02	15.2	0.41	12.8	7.49	2.79	0.06	0.52	
	T_{liq}	T_{sol}	T	ρ_l	ρ_b	μ_l	c_l	L_l	$X'(T)$			
Lava parameters	°C	°C	°C	kg/m^3	kg/m^3	Pa s	J/kg °C	J/kg	°C^{-1}			
	1270	1150	1270	2820	2820	2.32	1560	5.28E+05	−1/625			
			1260	2810	2814	3.68	1560	5.24E+05				
			1250	2800	2810	5.95	1560	5.19E+05				
	T_{mg}	T_{vap}	ρ_g	μ_g	c_g	L_g	L_{vap}	k_g	f_w			
Substrate parameters	°C	°C	kg/m^3	Pa s	J/kg °C	J/kg	J/kg	J/m s °C	(0–1)			
	1080	311	3180	35.6	1560	4.42E+05	2.50E+06	1.00	0–0.250			
	f_v	ρ_{vap}	c_{vap}		T_a	P_{atm}	g	h	α			
Lava bubbles and other physical parameters	vol %	kg/m^3	J/kg °C		°C	kPa	m/s^2	m	°			
	30.0–65.0	1.00	2630		−59.0	6.40E−06	3.74	20.0	0.0360 (av.)			
								30.0				
								40.0				
								68.0	0.0600 (prox.)			
								80.0				

Liquidus temperature, T_{liq}, was calculated using MELTS [*Ghiorso and Sack*, 1995]; solidus temperature, T_{sol}, is from *Arndt* [1976]; T is lava eruption temperature; liquid density, ρ_l, was calculated using the method of *Bottinga and Weill* [1970], with the coefficients of *Mo et al.* [1982]; bulk density, ρ_b, as a function of pressure, temperature, and composition was calculated by the method of *Mo et al.* [1982]; liquid viscosity, μ_l, was calculated using the method of *Shaw* [1972]; specific heat, c_l, was calculated using the method of *Lange and Navrotsky* [1992]; heat of fusion, L_l, is approximated from data of *Navrotsky* [1995]; $X'(T)$ is the increasing volume fraction of olivine crystals with decreasing temperature.

Unless otherwise specified, the following variables are from *Williams et al.* [1998]. T_{mg} is melting temperature of basalt substrate [*Navrotsky*, 1995]; T_{vap} is temperature of vaporization of substrate water; ρ_g is density of basalt substrate; μ_g is viscosity of basalt substrate, calculated using the method of *Shaw* [1972]; c_g is specific heat of basalt substrate, from *Williams et al.* [2005]; L_g is heat of fusion of basalt substrate [*Navrotsky*, 1995]; L_{vap} is heat of vaporization of substrate water, calculated by the method of *Huppert and Sparks* [1985]; k_g is thermal conductivity of basalt substrate; f_w is volume fraction of water in substrate pore space; f_v is volume fraction of bubbles in the lava; ρ_{vap} and c_{vap} are density and specific heat of water vapor, from *Serway and Jewett* [2014]; T_a is ambient temperature at Martian surface; g is acceleration due to gravity at Martian surface; h is lava thickness; α is average ground slope for the entire flood lava (av.) and at proximal Athabasca (prox.).

flow moves downstream, and (3) the flow thickness increase as velocity decreases (thickness is used as a proxy for flux, which is conserved as the flow moves downstream). Several algorithms are used to calculate initial values of important temperature- and composition-dependent thermal-physical lava properties, including solidus and liquidus temperatures, liquid density and viscosity, lava-specific heat, and thermal conductivity. However, these algorithms require an initial lava major oxide composition, and a set of topographical parameters associated with the flow is also required to run the model. We have listed the complete set of input values of the *Williams et al*. [2005] model, including the composition, the thermal/rheological properties of lava and substrate, and the topographic parameters in Table 1. The crystallization sequence of the Adirondack basalt was modeled with MELTS and its viscosity accurately determined by *Chevrel et al*. [2014]. Among the thermal/rheological properties, the liquidus temperature (T_{liq}) was calculated using MELTS [*Ghiorso and Sack*, 1995] and the solidus temperature (T_{sol}) was taken from the experimental data of *Arndt* [1976]. The initial lava pressure—at time of eruption—was assumed to be equal to the environmental pressure on the Martian surface, i.e., 6.40×10^{-6} kbar. Liquid density (ρ_l) was calculated using the method of *Bottinga and Weill* [1970], and density changes as a function of evolving pressure, temperature, and composition were obtained by adopting the partial molar volume coefficients of *Mo et al*. [1982]; liquid viscosity (μ_l) was calculated using the method of *Shaw* [1972]; specific heat (c_l) was calculated from the heat capacity data of *Lange and Navrotsky* [1992]; and the temperature-dependent heat of fusion (L_l) is approximated using expressions for the mineral representing the highest volume percentage of the rock (here forsteritic olivine, from *Navrotsky* [1995]). Among the topographic parameters, two values of ground slope were considered, one referring to the proximal portion of the Athabasca channel and the other averaged over the entire length of the 300 km long channel ($\alpha = 0.06°$ and $\alpha = 0.036°$, respectively, the latter from *Jaeger et al*. [2010]).

The initial values shown in Table 1 are used in a series of auxiliary equations to calculate additional lava properties at the vent and at progressively increasing distances downstream. Lava crystallinity X is given by the ratio of the degree of undercooling divided by the range of crystallization, as follows:

$$X = \frac{(T_{liq} - T)}{(T_{liq} - T_{sol})} \tag{1}$$

in which T_{liq} is the liquidus temperature, T_{sol} is the solidus temperature, and T is lava temperature at the vent and then at progressively increasing downstream distances. Crystallinity, expressed as a total volume fraction, is calculated by assuming constant liquidus and solidus temperatures rather than a range of values, and a linear growth (in the crystal fraction) with cooling, the latter assumption giving an adequate approximation for lavas crystallizing a single silicate phase (olivine) [*Williams et al*., 2000a]. Crystal growth and the presence of bubbles (which will be discussed later) in the lava interior are the only parameters in calculating bulk viscosity, although the strength of the crust may also influence the bulk motion of the flow. The bulk viscosity, μ_b, is expressed as a function of the initial liquid viscosity, μ_l, by the Roscoe-Einstein equation (2a):

$$\mu_b = \mu_l \left(1 - \frac{X}{0.600}\right)^{-2.5} \tag{2a}$$

$$\mu_b = \mu_l \exp\left[2.50 + \left(\frac{X}{0.600 - X}\right)^{0.48}\right] \frac{X}{0.600} \tag{2b}$$

at crystal fractions $X < 0.3$ and by the *Pinkerton and Stevenson* [1992] relation (2b) at crystal fractions $X > 0.3$. Equations (2a) and (2b) assume that the crystals remain in suspension during flow emplacement, which is strongly indicated during turbulent flow [*Huppert and Sparks*, 1985]. Following this, flow velocity u, friction coefficient λ, and Reynolds number Re (equations (3a)–(3c)) are calculated iteratively:

$$u = \sqrt{\frac{4gh\sin(\alpha)}{\lambda}} \tag{3a}$$

$$\lambda = [0.790 \ln(\mathrm{Re}) - 1.64]^{-2} \tag{3b}$$

$$\mathrm{Re} = \frac{2\rho_b u h}{\mu_b} \tag{3c}$$

in which g is acceleration due to gravity, h is flow thickness, α is ground slope, and ρ_b is the bulk density of the flow (liquid + crystals). The value Re = 2000 is chosen as the theoretical limit on turbulent flow in conduits.

Another calculated composition-dependent thermal-physical property of the lava is the Prandtl number, Pr, the ratio of momentum diffusivity to thermal diffusivity (4).

$$\mathrm{Pr} = \frac{c_l\,\mu_b}{k_{eff}} \tag{4}$$

In this expression, c_l is lava-specific heat, and k_{eff} is the effective lava thermal conductivity in the thermal boundary layers at the base and top of the flow, respectively (equations (5a) and (5b)) [*Williams et al.*, 1998]. The effective thermal conductivity is expressed as

$$k_{eff} = \frac{0.00130\,(T - T_{mg})}{\ln\left(\frac{2.16 - 0.00130\,T_{mg}}{2.16 - 0.00130\,T}\right)} \tag{5a}$$

$$k_{eff} = \frac{0.00130\,(T - T_{sol})}{\ln\left(\frac{2.16 - 0.00130\,T_{sol}}{2.16 - 0.00130\,T}\right)} \tag{5b}$$

In (5a), T_{mg} is the effective melting temperature of the substrate (which for a given value of viscosity of the melted substrate, μ_g, maximizes thermal erosion). Unlike *Hulme* [1973] and *Huppert and Sparks* [1985], *Williams et al.* [1998] adopt more than one expression for the convective heat transfer coefficient (h_T), and we use here one that includes the effects for turbulent pipe flows:

$$h_T = \frac{0.0270\,k_{eff}\,\mathrm{Re}^{4/5}\,\mathrm{Pr}^{1/3}}{h}\left(\frac{\mu_b}{\mu_g}\right)^{0.14} \tag{6}$$

in which μ_g is calculated as a function of T_{mg} and is equal to 35.6 Pa s for a substrate that is basaltic in composition [*Williams et al.*, 1998]. The ratio of the lava bulk viscosity to the viscosity of the melted substrate in (6) has the effect of reducing heat transfer compared to that found in fluids with constant physical properties.

Lava thermal erosion rate, u_m, as modified from *Huppert and Sparks* [1985], is given by

$$u_m = \frac{h_T(T - T_{mg})}{E_{mg}} \tag{7a}$$

$$E_{mg} = \rho_g\left[c_g(T_{mg} - T_a) + L_g\right] \tag{7b}$$

in which E_{mg} is the energy required to melt the substrate, ρ_g is substrate density, c_g is substrate-specific heat, T_a is ambient temperature of the surface, and L_g is heat of fusion required to melt the substrate. Lava thermal erosion rates enable estimates of erosion depth to be made by simply multiplying erosion rate values (varying as a function of distance from lava source) by the elapsed time t since flow began, assuming steady-flow conditions. The erosion rate is used to calculate the degree of contamination, as a volume fraction, of the lava by assimilated substrate, $S(x)$, given by

$$S(x) = 1 - \frac{Q_0}{Q(x)} \tag{8a}$$

$$Q(x) = Q_0 + \int_0^x u_m\,dx \tag{8b}$$

in which Q_0 is the initial flow rate and $Q(x)$ is the flow rate at any given distance (x) from the source. Finally, the mass expressions

$$M_{new} = M_{old}(1 - \Delta S) + M_{asm}(\Delta S) \text{ and} \tag{9a}$$

$$M_{new} = M_{old}(1 - \Delta X) + M_{olv}(\Delta X) \tag{9b}$$

are used to calculate the compositional change in the liquid lava due to the assimilation of thermally eroded substrate S and the crystallization of minerals (olivine) as a mole fraction, X, at each model distance increment. Here M_{new} is the major oxide composition of the lava at the current distance from the source, M_{old} is the major oxide composition of the lava at the previous distance increment, M_{asm} is the major oxide composition of the substrate, and M_{olv} is the olivine major oxide composition. Equation (9b) is used in conjunction with partition coefficient and stoichiometric algorithms to calculate M_{olv} at each model increment of distance. The newly calculated lava composition from (9b) is then used to recalculate the temperature- and composition-dependent thermal, rheological, and fluid dynamic properties of the lava at each distance increment downstream.

Lava temperature is the key parameter that advances the model, and it decreases as the flow moves downstream. This model of lava cooling with distance is given by the following first-order ordinary differential equation (modified from *Huppert and Sparks* [1985]):

$$\rho_b c_l h u \frac{dT}{dx} = -h_T(T - T_{mg}) - h_T(T - T_{sol}) - \frac{\rho_b c_l h_T (T - T_{mg})^2}{E_{mg}} + \rho_b c_l h u \frac{dT}{dx} \frac{L_l X'(T)}{c_l} \quad (10)$$

in which L_l is the lava heat of fusion and $X'(T)$ represents the increasing volume fraction of olivine crystals in the lava with decreasing temperature, equal to $-1/625°C^{-1}$ (derived from the slope of the liquidus, Figure 2) [*Usselman et al*., 1979]. Because the physical properties of the lava are changing with distance, (10) must be solved at each increment of distance from the eruption source using a fourth-order Runge-Kutta numerical method. Once a new temperature (from equation (10)) and a new lava composition (from equations (9a) and (9b)) are obtained, the new thermal, rheological, and fluid dynamic parameters are calculated at that distance. In doing so, the physical and geochemical evolution of the lava flow at progressively increasing downstream distances from the source is simulated.

The effect of bubbles on the emplacement of the lava is also assessed in the *Williams et al*. [2000a] model. In order to account for such an effect, the bulk density, "effective" viscosity, and specific heat equations found in *Williams et al*. [2000a] have replaced their counterpart expressions within the sequence of algorithms mentioned above. The term "effective" implies that liquid, solid (olivine crystals), and gas phases (H_2O vapor) may coexist in the lava during flow emplacement. By defining a parameter for the fraction of the lava consisting of bubbles (f_v), the effect on these physical properties can be assessed by the following equations:

$$\rho_{eff} = f_v \left(\rho_{vap}\right) + (1 - f_v)\rho_b \quad (11)$$

$$c_{eff} = f_v \left(c_{vap}\right) + (1 - f_v)c_l \quad (12)$$

$$\mu_{eff} = \mu_b \left[\frac{1}{1 - (1.30\, f_v)^{1/3}}\right] \quad (13)$$

in which the subscript eff refers to liquid plus crystals and/or bubbles, vap refers to the volatile gas in the bubbles, b refers to bulk (liquid plus crystals), and l refers to liquid. Equation (13), which is recommended by *Pinkerton and Stevenson* [1992] to assess the effect of bubbles on lava viscosity, is from *Sibree* [1934] and is valid for foams with values of f_v up to 75%.

To simulate thermal erosion over an unconsolidated substrate, the *Williams et al*. [1998, 2005] model considers the possible effects of particle disaggregation due to melting of ice and vaporization of intergranular water. Once intergranular water reaches the boiling point, it vaporizes. Because water expands as it changes phase from liquid to vapor, the expansion may fragment the unconsolidated substrate and lead to mechanical mixing (mechanical erosion) with the lava before subsequent melting and assimilation (thermal erosion). A similar process of thermomechanical erosion can be described by energy conservation, as follows:

$$\rho_b c_l h \frac{dT}{dt} = -h_T(T - T_{vap}) - h_T(T - T_{sol}) - \frac{h_T(T - T_{vap})E_{hg}}{E_{dg}} + \rho_l h \frac{dT}{dt} L_l X'(T) \quad (14a)$$

in which E_{dg} is the energy required to disaggregate the ground, given by

$$E_{dg} = (1 - f_w)\rho_g c_g (T_{vap} - T_a) + f_w \rho_w \left[c_w (T_{vap} - T_a) + L_{vap}\right] \quad (14b)$$

and E_{hg} is the energy required to heat the disaggregated ground up to the lava temperature:

$$E_{hg} = (1 - f_w)\rho_g \{c_g (T - T_{vap}) + L_g\}\, f_w\ \rho_w\, c_{vap} (T - T_{vap}) \quad (14c)$$

in which f_w is the volume fraction of ice/water in the substrate, ρ_w and c_w are the density and specific heat of water/ice in the substrate, respectively, T_{vap} is the temperature at which all substrate water is vaporized, and L_{vap} is the latent heat of vaporization of water. Finally, the erosion rate is given by

$$u_m = \frac{h_T(T - T_{vap})}{E_{dg}} \quad (15)$$

This erosion rate determines the upflow velocity of steam produced by vaporization of intergranular ice/water. The model predicts that particles up to the size of very fine sand (<0.1 mm) can be physically removed from the substrate, i.e., mechanically eroded, in this manner. Once again, the calculated lava

thermal erosion rate and degree of contamination of the lava by assimilated substrate enable estimates of erosion depth to be made by simply multiplying erosion rate values (varying as a function of distance from the lava source) by the elapsed time, *t*, since flow began, assuming steady-flow conditions.

2.2. Model Assumptions

The user-friendly interface of the C-written code makes the *Williams et al*. [1998] model especially adaptable to simulate various eruption conditions and planetary environments. Key input parameters of the model include (1) the major oxide composition of the erupted lava and underlying substrate, (2) an initial value of lava thickness, (3) amounts of ice in the substrate of 0 vol % (consolidated substrate) and 25 vol % (unconsolidated substrate), and (4) substrate slope prior to any erosion.

Both lava and substrate are assumed to have a composition similar to that measured by Spirit at Gusev crater. For a reduced Adirondack melt at the liquidus temperature of 1270°C (1543 K), we have calculated a liquid viscosity of ~4.8 Pa s, by using equation (3) from *Chevrel et al*. [2014]. At the same temperature, the liquid viscosity had been previously estimated to be 2.8 Pa s [*Greeley et al*., 2005], and we have also found a value of 2.32 Pa s by using the MELTS program [*Ghiorso and Sack*, 1995]. We have chosen the last value because lower flow viscosities maximize erosion rates and depths of the lava substrate, holding other factors equal. However, no real constraint on the eruption temperature exists [*Jaeger et al*., 2010], which has led us to choose three values of eruption temperature (1270°C, 1260°C, and 1250°C) to investigate the extent to which a similar temperature variation may affect the key physical parameters of the flow along with erosion rates and depths. The *Williams et al*. [1998] model shows that, if the lava temperature decreases below 1250°C, the dynamic viscosity of the flow increases much faster as a function of distance from the lava source. Specifically, once an eruption temperature of 1243°C is chosen, the model stops producing turbulent flow scenarios. Also, we do not choose a temperature higher than 1270°C, because this value represents the liquidus temperature for the lava composition of interest and no author has suggested that superheated lavas were likely erupted at Athabasca. With bubbles and cooling (and crystallization), *Greeley et al*. [2005] suggested that a value of 50 Pa s might be more realistic for the bulk viscosity of the lava during emplacement. To assess the effect of bubbles on the emplacement of the lava as well as the ability of the flow to erode the substrate, we have followed the methodology adopted by *Williams et al*. [2000a], and let the Athabasca Valles turbulent lava contain 30–65% by volume of bubbles at the vent. The presence of bubbles in the lava decreases bulk lava density and increases flow viscosity at low strain rates [*Pinkerton and Stevenson*, 1992], whereas at high strain rates bubbles will deform, reducing bulk flow viscosity [*Spera et al*., 1988]. More recently, the effects of gas volume fractions and frequency of oscillation on the elastic and viscous components of bubble deformation were investigated by *Llewellin et al*. [2002] and are discussed more in depth in section 4. In the case of turbulent flow, high strain rates should be expected, but this is a scenario for which the effect of bubbles has not yet been assessed. To account for such an effect, the bulk density, effective viscosity and specific heat equations found in *Williams et al*. [2000a] are now used within the sequence of algorithms mentioned in section 2.1.

For the very wide (~39 km in diameter) and shallow (~80–100 m deep) proximal Athabasca channel, the value of the hydraulic radius closely approximates flow thickness [*Shaw and Swanson*, 1970]. The hydraulic radius of the lava is taken to be in the range 20–68 m, the latter value matching previously estimated maximum volumetric flux rates [2.0×10^{-2} km^3 s^{-1}, from *Jaeger et al*., 2010], although we include results for an 80 m thick flow. Observations from digital terrain models indicate that the deepest parts of the channel center are as much as 100 m below the observed high-lava marks [*Jaeger et al*., 2010].

We explore the effect of the substrate characteristics on the lava flow propagation by considering two types of substrate: dry and consolidated, and ice rich and unconsolidated. Rootless cones provide evidence that water or ice was present in the shallow subsurface at the time of the eruption [*Jaeger et al*., 2007]. To simulate thermal erosion of an unconsolidated substrate, the *Williams et al*. [1998, 2005] model accounts for the possible effects of particle disaggregation (i.e., mechanical erosion) caused by melting of ice and vaporization of intergranular water; the energy required to vaporize the water and disaggregate the ground is considered in the model. All of the water is assumed to be vaporized in the process, with the maximum volume fraction of water present in the substrate pore space being equal to 25%.

Data made available by the Mars Orbiter Laser Altimeter (MOLA) instrument aboard the Mars Global Surveyor spacecraft, with a vertical precision to within 30 cm in the vertical dimension [*Zuber et al*., 1992], enabled determination of the average slope of the substrate. The value is calculated to be ~0.06° at proximal

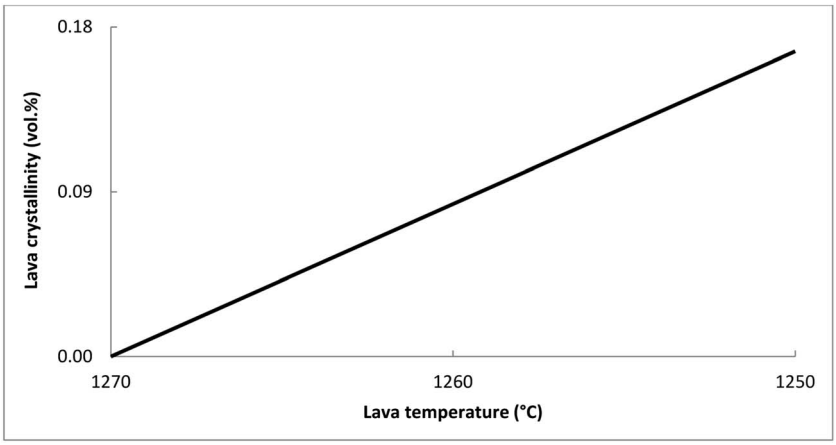

Figure 3. Lava crystallinity is calculated by assuming constant liquidus and solid temperatures, and a linear growth of crystals occurs with cooling. This result is consistent with crystallizing a single silicate phase (olivine).

Athabasca, but we also adopt the value of 0.036°, which is averaged across the entire length of the Athabasca channel [*Jaeger et al*., 2010], to test the effect of slope on erosion rates and depths. Along with all the important temperature- and composition-dependent thermal-physical properties of the lava, the model generates flow velocities and flow thicknesses, which are then multiplied by channel width to obtain 3-D flow rates. From these, we derive an estimate of flow duration by using the available range of flow volumes obtained from *Jaeger et al*. [2010].

3. Results

Results are grouped in two sets: one set assesses the influence of different eruption temperatures and lava thicknesses on erosion rates and erosion depths into the substrate; the other set, while keeping the eruption temperature the same, describes the extent to which the likely presence of bubbles in the lava may affect its viscosity and thereby lead to a reduced amount of thermal erosion.

3.1. Erosion Rates and Depths for Three Eruption Temperatures at Proximal Athabasca

Crystallization associated with cooling has a strong impact on magma viscosity [*Lejeune and Richet*, 1995; *Caricchi et al*., 2007; *Champallier et al*., 2008]. Figure 3 shows the described linear relationship between crystal growth and decreasing lava temperatures. As the lava is erupted at or reaches a temperature of 1250°C, ~17 vol % of the original melt is crystallized. We used the MELTS program [*Ghiorso and Sack*, 1995] for the given initial magma composition. Currently, redox conditions of martian magmas are poorly known, because of (1) the inconsistency between the amounts of magnetite found in basaltic rocks at Gusev Crater [*Morris et al*., 2008] and those found in martian meteorites [*Stolper and McSween*, 1979; *Treiman*, 2005] and (2) the current, albeit limited, knowledge of iron redox equilibria and phase relations in martian magmas. Thus, a range of oxygen fugacity conditions were considered for our MELTS runs. Results confirm that olivine is the

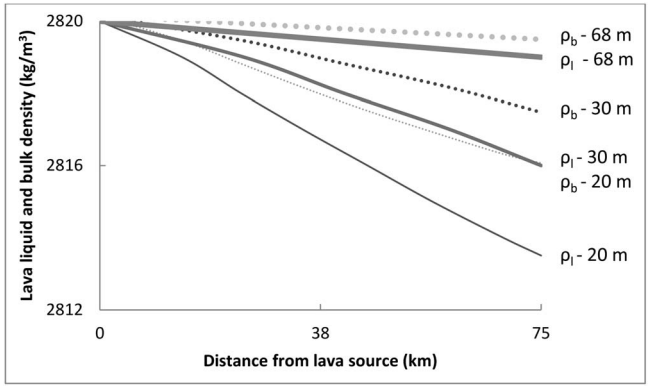

Figure 4. Lava liquid (ρ_l) and bulk (ρ_b) densities plotted against distance, out to 75 km from the lava source, here defined as proximal Athabasca. Eruption temperature, T_e, is equal to 1270°C (liquidus). Flows 20 and 30 m thick are accompanied by a greater decrease in density with increasing downstream distance relative to a 68 m thick flow, and bulk density values are always higher than liquid values for the same flow thickness and at similar downstream distances.

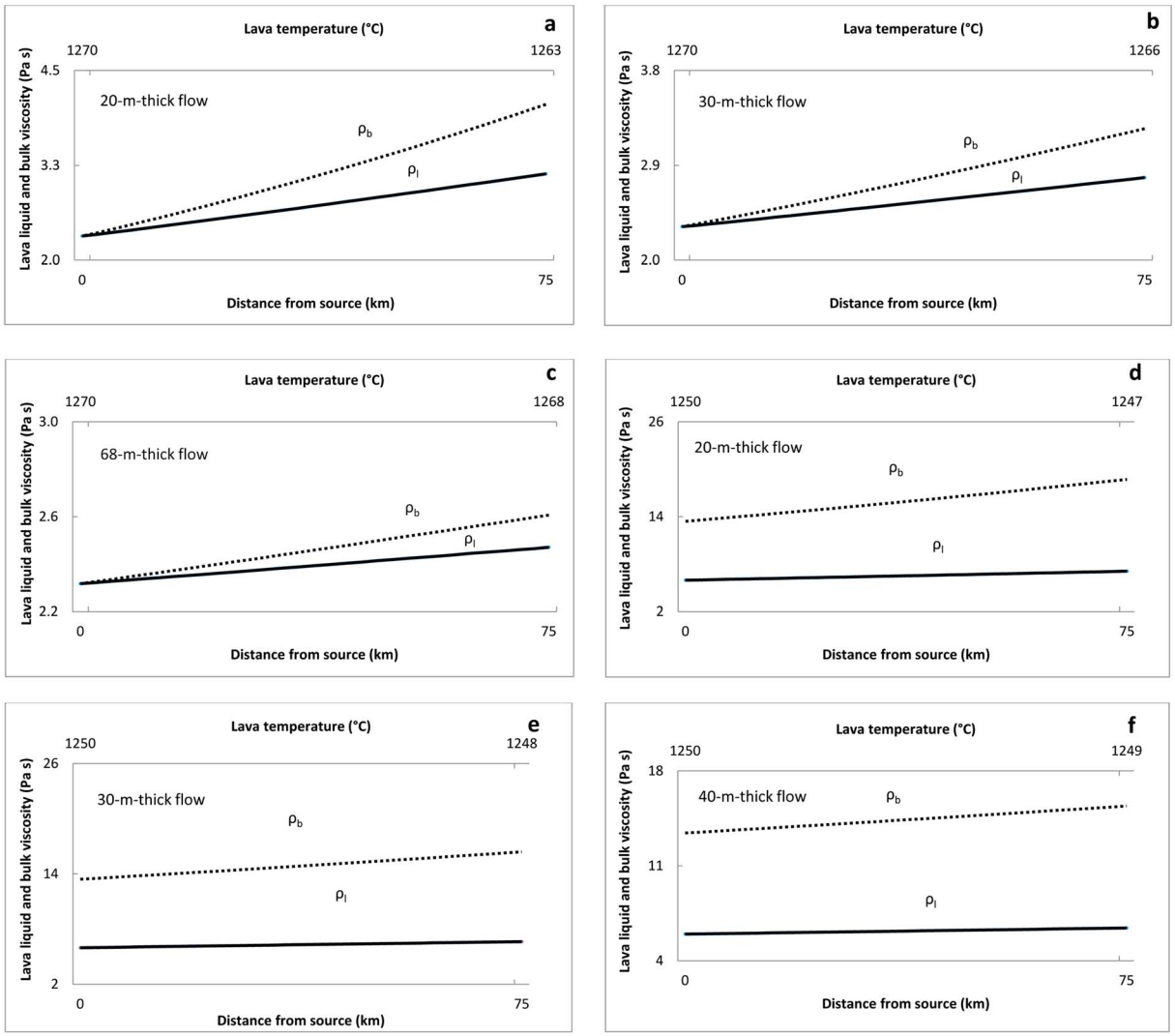

Figure 5. (a) Liquid (ρ_l) and bulk (ρ_b) flow viscosities for a 20 m thick flow, plotted versus distance from lava source and decreasing lava temperatures at proximal Athabasca. Temperature of eruption is 1270°C (liquidus). The bulk viscosity of the flow increases by a factor of 1.8 from its original value, and much faster than liquid viscosity. Lava temperatures decrease by ~7°C, over the 75 km long proximal region. (b) Liquid (ρ_l) and bulk (ρ_b) flow viscosities for a 30 m thick flow, plotted against distance from lava source and decreasing lava temperatures at proximal Athabasca. Temperature of eruption is 1270°C (liquidus). The bulk viscosity of the flow increases by a factor of 1.4 from its original value, and lava temperatures decrease by ~4°C, over the proximal portion of the Athabasca channel. (c) Liquid (ρ_l) and bulk (ρ_b) flow viscosities for a 68 m thick flow plotted against distance from lava source and decreasing lava temperatures at proximal Athabasca. The lava is erupted at the liquidus temperature (1270°C). The bulk viscosity of the flow increases less than for a 20 m thick flow—by up to a factor of 1.1—and shows a trend of variation closer to that of the liquid viscosity. Lava temperatures decrease by less than 2°C, over the same distance. (d) Liquid (ρ_l) and bulk (ρ_b) flow viscosities for a 20 m thick flow, plotted against distance from lava source and decreasing lava temperatures at proximal Athabasca. Temperature of eruption is 1250°C. Because of the lower eruption temperature, initial flow viscosities are much higher than those associated with a flow erupted at the liquidus temperature. The bulk viscosity increases by a factor of 1.4 from its original value—from 13.4 to 18.7 Pa s—and lava temperatures decrease by ~3°C, over the proximal portion of the Athabasca channel. (e) Liquid (ρ_l) and bulk (ρ_b) flow viscosities for a 30 m thick flow plotted versus distance from lava source and decreasing lava temperatures at proximal Athabasca. Temperature of eruption is 1250°C. Bulk and liquid viscosities increase by only a factor of ~1.2 and 1.1, respectively, from their initial values at the lava source. (f) Liquid (ρ_l) and bulk (ρ_b) flow viscosities for a 40 m thick flow, plotted against distance from lava source and decreasing lava temperatures at proximal Athabasca. Temperature of eruption is 1250°C. The greater thickness promotes efficient mixing within the flowing lava and causes both liquid and bulk viscosities to increase within a factor of 1.15 from their initial values. Lava temperatures decrease by less than 2°C, over the proximal portion of the Athabasca channel.

only crystallizing phase, but the percentage of crystals forming as the temperature of the flowing lava decreases to 1250°C is always < 4 vol %. As a result, the bulk viscosity of the flowing lava is, on average, ~30% lower than that obtained by the *Williams et al*. model, which accommodates for assimilation of thermally eroded substrate within the flowing lava, the process that is likely responsible for the higher viscosity values.

Table 2. Output Eruption Parameters, Shown as a Function of Lava Flow Rates and Flow Thickness, at Proximal Athabasca[a]

T_e (°C)	r_{h_0} (m)	T_{75} (°C)	r_{h75} (m)	ρ_{b_av} (kg/m^3)	μ_{l_0} (Pa s)	μ_{l_75} (Pa s)	μ_{b_0} (Pa s)	μ_{b_75} (Pa s)	u_0 (m/s)	u_75 (m/s)	Re$_0$ (#)	Q_{pr} (km^3/s)
1270	20.0	1263	20.8	2817	2.32	3.14	2.32	4.06	4.51	4.35	2.20E+05	3.52E−03
1270	30.0	1266	30.7	2818	2.32	2.78	2.32	3.25	5.89	5.77	4.30E+05	6.90E−03
1270	40.0	1267	40.6	2819	2.32	2.63	2.32	2.93	7.10	7.00	6.91E+05	1.11E−02
1270	68.0	1268	68.5	2819	2.32	2.47	2.32	2.61	9.96	9.90	1.65E+06	2.64E−02
1270	80.0	1269	80.4	2820	2.32	2.44	2.32	2.55	11.0	11.0	2.15E+06	3.44E−02
1260	20.0	1255	20.7	2807	3.68	4.65	5.45	8.45	4.26	4.12	9.32E+04	3.33E−03
1260	30.0	1257	30.6	2808	3.69	4.25	5.46	7.11	5.58	5.48	1.82E+05	6.53E−03
1260	40.0	1257	40.5	2809	3.69	4.07	5.47	6.56	6.74	6.66	2.92E+05	1.05E−02
1260	68.0	1258	68.4	2809	3.69	3.88	5.47	6.00	9.49	9.44	6.97E+05	2.52E−02
1260	80.0	1259	80.4	2810	3.69	3.84	5.47	5.89	10.5	10.5	9.09E+05	3.29E−02
1250	20.0	1246	20.6	2798	6.11	7.25	14.1	19.6	3.96	3.86	3.60E+04	3.10E−03
1250	30.0	1248	30.5	2798	6.11	6.78	14.1	17.2	5.22	5.14	7.03E+04	6.11E−03
1250	40.0	1248	40.5	2799	6.11	6.57	14.1	16.2	6.32	6.26	1.13E+05	9.87E−03

[a]The suffixes "0" and "75" refer to the lava source region and a downstream distance of 75 km, respectively; "av" means averaged across section length; "pr" stands for proximal.

Figures 4 and 5 show how the density and viscosity of the flow vary as a function of decreasing lava temperatures and increasing downstream distances. Figure 4 shows how lava thickness and downstream distances affect the rate of variation of both liquid and bulk flow densities. The eruption temperature is held at 1270°C (liquidus). For a 20 m thick lava flow, the liquid density decreases by ~0.25% from its initial value of 2820 kg/m^3 over the 75 km long proximal channel, whereas it remains almost equal to its initial value of 2820 kg/m^3 over the same distance, for a 68 m thick flow. Average bulk densities range from 2820 kg/m^3 (for an 80 m thick flow erupted at the liquidus temperature) to ~2800 kg/m^3 (for a 20 m thick flow and a lava temperature in the range 1250°C–1246°C) (Table 2).

Table 2 shows that bulk viscosities never exceed ~20 Pa s, for the same interval of lava temperatures and a flow thickness of 20 m. This likely results from our model assumption of a thermally mixed interior, consistent with a fully turbulent regime, with Reynolds numbers in the range 3.60×10^4–2.15×10^6, the higher values being associated with liquidus lava temperatures ($T = 1270$°C) and flows thicker than 30 m. Figures 5a–5f show the control exerted by temperature and distance from lava source on flow viscosity. Flow viscosity and lava thickness increase as lava temperatures decrease with increasing distance from the lava source. Figures 5a–5c refer to an eruption temperature of 1270°C (liquidus) and lava flow thicknesses in the range of 20–68 m. Figure 5a shows that flow viscosities increase faster for a 20 m thick flow—by a factor of ~1.8 or from ~2.3 to ~4.1 Pa s through the end of proximal—which helps explain why turbulent flow conditions are more easily achieved and maintained by thicker lavas, as shown in Figure 6. Lava temperatures decrease faster for 20 m thick flows—by ~7°C, over the 75 km long proximal channel—and by less than 2°C, over the same distance, and for a 68 m thick flow. Figures 5d–5f show the impact of a lower eruption temperature of 1250°C on the rate of variation in viscosity with increasing

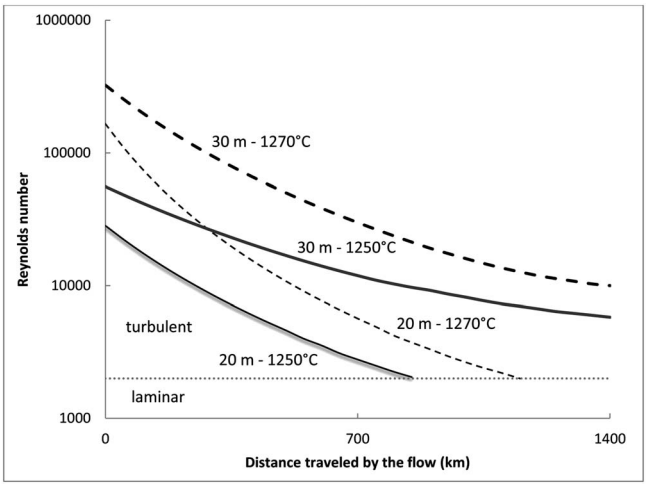

Figure 6. Reynolds number of the flow plotted against total distance traveled by the flow (1400 km) [after *Jaeger et al.*, 2010]. For initial eruption temperatures of 1270°C and 1250°C, a 30 m thick lava flow is shown to have flowed turbulently for all its length. All values were obtained by assuming an average slope of the ground of 0.036°, which suits the entire Athabasca channel [*Jaeger et al.*, 2010], and were used to calculate average flow rates and flow durations for the entire Athabasca flood lava.

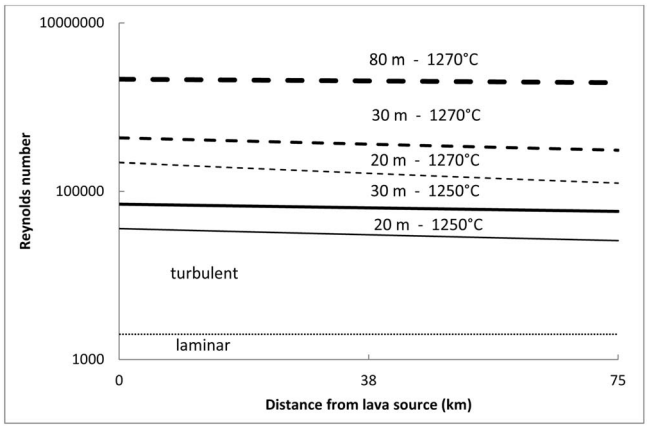

Figure 7. Reynolds number of the flow plotted against distance from lava source at proximal Athabasca. Values refer to lava thicknesses in the range 20–80 m, and eruption temperatures of 1270°C and 1250°C. Flow conditions are fully turbulent.

downstream distances and decreasing lava temperatures, for 20–40 m thick lava flows. Liquid and bulk viscosities increase by up to a factor of ~1.2 and 1.4, respectively, and lava temperatures decrease by up to ~3°C (for 20 m thick flows) and ~1°C (for 40 m thick flows). For a 20 m thick flow, bulk viscosity values increase from 13.4 to 18.7 Pa s, i.e., by a factor of ~1.4, this being likely a consequence of the presence of crystals at time of eruption, compared to the liquidus temperature scenario.

At proximal Athabasca, the measured average preflow slope of ~0.06° is responsible for the higher flow velocities—in the range 4.51–11.0 m/s—and flow rates that reach 3.44×10^{-2} km^3/s (Table 2). Flow conditions were likely fully turbulent, across the considered range of lava thicknesses and eruption temperatures (see Figure 7). By comparison, Table 3 lists the key parameters concerning the other portions of the Athabasca main channel, which are characterized by a lower underlying slope (mean value 0.036°, from *Jaeger et al*. [2010]) and which enabled determination of average flow rates lower than those obtained at proximal Athabasca by a factor of ~1.3 and total flow durations ranging from 2.22 to 37.2 days and obtained from 80 m and 20 m thick lava flows, respectively.

The calculated flow velocities fall within previously estimated values [*Jaeger et al*., 2010] for thicknesses ≥30 m. Lava temperatures decrease by <8°C from initial eruption values over the 75 km long proximal Athabasca channel, with the largest temperature drop occurring for a 20 m thick flow erupted at the liquidus temperature (1270°C). Therefore, a 20 m thick lava flow is unlikely to have flowed fully turbulently to a distance of ~1400 km from the vent (Table 3 and Figure 6).

Table 3 suggests that, on average, a flow ≥30 m thick may have flowed turbulently as far as ~1400 km from the vent, thus covering the total distance traveled by the Athabasca flood lava (see also Figure 6). The actual flow emplacement was likely more complex due to branching, ponding, and changes in slope along the flow. Calculated effusion rates vary by a factor of ~8 for thicknesses in the range 20–68 m and up to a factor of ~10, if the bankfull flow thickness of 80 m is included (Tables 2 and 3). Flow rates increase mainly as a function of increasing flow thickness and, to a lesser extent, increasing lava temperature (because increasing lava temperature decreases the bulk flow viscosity). The duration of the flow is necessarily approximate because

Table 3. Output Eruption Parameters, Shown as a Function of Lava Flow Rates and Flow Thickness, for the Entire Athabasca Valles Flood Lava[a]

T_e (°C)	r_{h_0} (m)	μ_{l_0} (Pa s)	μ_{b_0} (Pa s)	u_0 (m/s)	$Re_{\_0}$ (#)	$Re_{\_1400}$ (#)	Q_{Ath} (km^3/s)	t_a (days)	t_b (days)
1270	20.0	2.32	2.32	3.40	1.65E+05	<2000	2.65E−03	21.8	32.7
1270	30.0	2.32	2.32	4.45	3.25E+05	1.00E+04	5.20E−03	11.1	16.7
1270	40.0	2.32	2.32	5.36	5.22E+05		8.36E−03	6.92	10.4
1270	68.0	2.32	2.32	7.54	1.25E+06		2.00E−02	2.89	4.34
1270	80.0	2.32	2.32	8.36	1.63E+06		2.61E−02	2.22	3.33
1260	20.0	3.60	5.22	3.21	7.33E+04	<2000	2.51E−03	23.1	34.6
1260	30.0	3.60	5.23	4.22	1.44E+05	8.44E+03	4.93E−03	11.7	17.6
1260	40.0	3.60	5.24	5.10	2.31E+05		7.96E−03	7.27	10.9
1260	68.0	3.60	5.24	7.20	5.52E+05		1.91E−02	3.03	4.55
1260	80.0	3.60	5.24	7.99	7.19E+05		2.49E−02	2.32	3.48
1250	20.0	5.95	13.4	2.98	2.84E+04	<2000	2.33E−03	24.8	37.2
1250	30.0	5.95	13.4	3.94	5.58E+04	5.80E+03	4.62E−03	12.5	18.8
1250	40.0	5.95	13.4	4.78	8.98E+04		7.46E−03	7.75	11.6

[a]The suffix "0" refers to the lava source region; "1400" refers to a downstream distance of 1400 km from the lava source; "Ath" stands for Athabasca.

Table 4. Maximum Erosion Rates and Depths of the Lava Substrate, at Proximal Athabasca and Downstream of Proximal Athabasca[a]

T_e (°C)	r_h (m)	u_m (m/day)	u_{m_ice} (m/day)	D_a (m)	D_{a_ice} (m)	D_b (m)	D_{b_ice} (m)	u_{m_ls} (m/day)	$u_{m\_ls\_ice}$ (m/day)	$D_{ls\_b\_ice}$ (m)
1270	20.0	0.173	0.230	3.76	5.01	5.64	7.52	0.138	0.183	6.00
1270	30.0	0.197	0.263	2.19	2.91	3.29	4.38	0.157	0.210	3.49
1270	40.0	0.216	0.288	1.49	1.99	2.24	2.99	0.172	0.230	2.39
1270	68.0	0.255	0.339	0.738	0.984	1.09	1.46	0.204	0.272	1.18
1270	80.0	0.267	0.357	0.588	0.785	0.882	1.18	0.214	0.286	0.950
1260	20.0	0.111	0.147	2.56	3.38	3.83	5.07	0.0901	0.119	4.13
1260	30.0	0.127	0.168	1.48	1.96	2.23	2.95	0.104	0.138	2.43
1260	40.0	0.139	0.184	1.02	1.34	1.52	2.01	0.114	0.150	1.64
1260	68.0	0.165	0.218	0.494	0.654	0.741	0.981	0.135	0.178	0.811
1260	80.0	0.173	0.229	0.398	0.527	0.606	0.803	0.142	0.188	0.653
1250	20.0	0.0675	0.089	1.67	2.20	2.51	3.31	0.0549	0.0722	2.69
1250	30.0	0.0777	0.102	0.971	1.28	1.46	1.92	0.0634	0.0835	1.57
1250	40.0	0.0855	0.113	0.667	0.878	0.992	1.31	0.0699	0.0921	1.07

[a]The suffix "ls" stands for lower slope of the ground (0.036°); "ice" indicates that 25% by volume of ice was present in substrate pore space at time of flow emplacement.

flow rate is expected to vary with time. As a result, the values examined in Table 3 are plausible average values. A roughly order-of-magnitude difference between peak and mean flux is observed for smaller terrestrial fissure eruptions [e.g., *Wadge*, 1981]. If a similar relationship existed for the Athabasca Valles lava flow, this would not only affect the erosion rate but also the spatial distribution of erosion, because higher fluxes would inundate and erode some areas that would be untouched at a lower eruption rate. If we assume an average flow thickness in the range 20–30 m [*Jaeger et al.*, 2010] and refer to the emplacement of the total flow to a distance of ~1400 km from the vent, we obtain flow durations in the range of ~11–37 days (Table 3), in agreement with previous results from *Jaeger et al.* [2010]. The 11 day time refers to a total lava volume of 5000 km^3, a flow thickness of 30 m and an eruption temperature of 1270°C (liquidus). If we assume that the total bubble-free lava volume ranged between 5000 and 7500 km^3, a flow that on average is 20 m thick and is erupted at a temperature of 1250°C will take three to five additional days to be emplaced, respectively, compared to a similar flow of identical thickness, which is erupted at a temperature of 1270°C.

Table 4 shows erosion rates and depths—where depth $u = 0$ represents the preflow surface—as a function of eruption temperature, flow thickness, and substrate slope. Calculated values range from a minimum of ~0.05 m/day, for a 20 m thick flow erupted at 1250°C with 0.036° slope, to a maximum of ~0.36 m/day, for an 80 m thick flow that is erupted at the liquidus temperature and is flowing over a substrate with 25% ice (by volume) and 0.06° slope. Higher lava temperatures generate greater erosion depths, and for a given lava thickness, depth values are always higher near the vent. At proximal Athabasca, they vary from a minimum of ~0.4 m—for an 80 m thick flow that is erupted at $T = 1260$°C and is emplaced in ~2 days (Table 3)—to a maximum of ~7.5 m—for a 20 m thick flow, erupted at the liquidus temperature and emplaced over an ice-rich substrate in ~33 days (Table 3). Outside the proximal region, both erosion rates and depths are lower due to the lower slope of the ground. Erosion depth values are a factor of ~1.3 lower than those found at proximal Athabasca and range from a minimum of ~0.7 m to a maximum of ~6.0 m for 80 m and 20 m thick flows, respectively. For a 20 m thick flow, a 20°C difference in eruption temperature

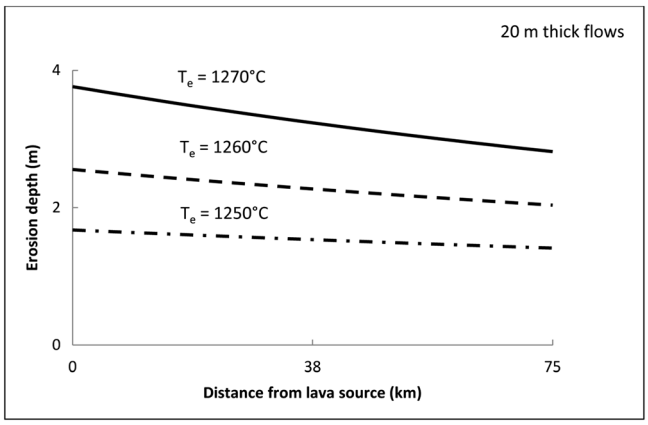

Figure 8. Influence of eruption temperature on erosion depth at proximal Athabasca. All values refer to a flow thickness of 20 m and are plotted against distance from lava source. Erosion depths were constrained by using the total flow volume estimate of 5000 km^3 [*Jaeger et al.*, 2010].

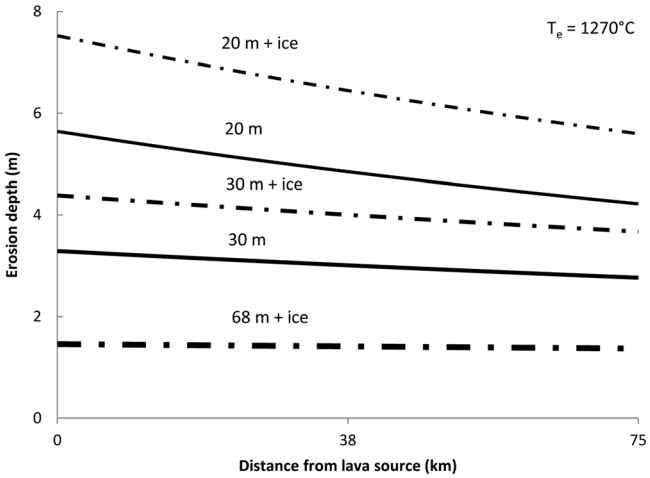

Figure 9. Erosion depths plotted against distance from lava source, for three lava flow thicknesses, at proximal Athabasca. All values refer to an eruption temperature of 1270°C. At this temperature, the erosion rate of the lava substrate is highest. Erosion depths were constrained by adopting the total flow volume estimate of 7500 km^3 [*Jaeger et al.*, 2010].

yields a ~2.1–4.2 m difference in erosion depth values at the lava source (see also Figure 8). Figure 9 shows maximum erosion depths—obtained by assuming a total flow volume of 7500 km^3—plotted against distance from lava source. The presence of ice in substrate pore space makes erosion depth values higher by a factor of 1.3, compared to a "dry" scenario. The 20 m thick flow erupted at a temperature of 1250°C, which is associated with the lowest erosion rate, and generated an erosion depth of ~3.3 m at the lava source (Table 4) in a period of ~37 days (Table 3). Importantly, flow duration is the most important parameter in determining the total amount of thermal erosion, and higher erosion rates are not necessarily associated with larger erosion depths—as shown in Tables 4 and 5. The 68 and 80 m thick flow units are capable of generating erosion depths ≤1 m, because the flow duration associated with those units is always <6 days (Tables 3 and 5).

In summary, our range of modeled erosion depths (~0.4–7.5 m), consistent with the proposed emplacement volumes and duration of the Athabasca flow, is far less than the depth of the channel (~35–100 m), regardless of the parameters used. Thus, our modeling suggests that thermal erosion does not appear to have had a major role in the formation of Athabasca Valles.

3.2. Lava Bubbles in the Flowing Lava and Their Impact on Erosion Rates and Depths

The likely occurrence of bubbles in the flow has the effect of either increasing or decreasing the "effective" viscosity of the flow, depending on bubble shapes and strain rates [*Llewellin et al.*, 2002]. We assume that lava viscosity increases with increasing proportions of gas bubbles in the flow. The eruption temperature is held constant at 1270°C, and the liquid bulk density and viscosity of the bubble-free flow remain constant and equal to 2820 kg/m^3 and 2.32 Pa s, respectively. Table 5 shows values of Reynolds number, flow rates, total volumes, and erosion rates and depths, which refer to lava flows of different thicknesses, containing 30–65% by volume of bubbles at the proximal Athabasca source region. Erosion depths were calculated by referring to total volumes of 6500, 7500, and 8250 km^3, which were obtained by adding the contribution of 30 vol %, 50 vol %, and 65 vol % of bubbles, respectively, to the original 5000 km^3 estimate.

Table 5. Erosion Rates and Depths, Shown as a Function of Bubble Content (H_2O Gas) in the Lava at the Source Region[a]

Bubbles (vol %)	r_{h_0} (m)	ρ_b (kg/m^3)	μ_{eff} (Pa s)	Re (#)	u (m/s)	Q (km^3/s)	V_{eff_0} (km^3)	t (days)	u_m (m/day)	u_{m_ice} (m/day)	D (m)	D_{ice} (m)
30.0	20.0	1970	8.60	3.38E+04	3.68	2.87E−03	6500	26.2	8.08E−02	1.08E−01	2.12	2.82
30.0	30.0	1970	8.60	6.72E+04	4.89	5.72E−03	6500	13.2	9.33E−02	1.24E−01	1.23	1.64
30.0	40.0	1970	8.60	1.09E+05	5.94	9.27E−03	6500	8.12	1.03E−01	1.37E−01	0.836	1.11
30.0	68.0	1970	8.60	2.64E+05	8.47	2.25E−02	6500	3.35	1.23E−01	1.64E−01	0.412	0.549
50.0	20.0	1410	17.3	1.03E+04	3.16	2.47E−03	7500	35.2	4.64E−02	6.19E−02	1.63	2.18
50.0	30.0	1410	17.3	2.08E+04	4.25	4.98E−03	7500	17.4	5.42E−02	7.22E−02	0.945	1.260
50.0	40.0	1410	17.3	3.40E+04	5.22	8.15E−03	7500	10.7	6.03E−02	8.04E−02	0.642	0.857
50.0	68.0	1410	17.3	8.34E+04	7.53	2.00E−02	7500	4.34	7.27E−02	9.69E−02	0.316	0.421
65.0	20.0	988	42.4	2.33E+03	2.51	1.96E−03	8250	48.8	2.25E−02	3.00E−02	1.10	1.47
65.0	30.0	988	42.4	4.84E+03	3.47	4.05E−03	8250	23.6	2.69E−02	3.59E−02	0.634	0.845
65.0	40.0	988	42.4	8.04E+03	4.32	6.74E−03	8250	14.2	3.03E−02	4.04E−02	0.430	0.573
65.0	68.0	988	42.4	2.02E+04	6.38	1.69E−02	8250	5.65	3.72E−02	4.96E−02	0.210	0.280

[a]The suffix "ice" indicates that 25% by volume of ice was present in substrate pore space at time of flow emplacement.

Total flow durations were obtained from the newly calculated flow rates and total volumes. A 30 m thick flow that contains 30 vol % bubbles is defined by a bulk density of 1970 kg/m^3, an effective viscosity of 8.60 Pa s, and a velocity of 4.89 m/s. This flow is calculated to erode the underlying substrate at rates of ~0.09–0.12 m/day, which are about half those that are obtained by a similar bubble-free flow, and gives maximum erosion depths of the substrate of ~1.2–1.6 m. A bubble-free flow of similar thickness would yield a maximum erosion depth of ~2.2–2.9 m. If the same flow contained 50 vol % bubbles, maximum erosion depths would be lower (~0.9–1.3 m). Thus, 30–50 vol % bubbles have the potential to reduce erosion depths by a factor of ~1.8–2.4, as compared to their bubble-free counterparts. In the case of a 30 m thick flow containing 65 vol % bubbles, maximum erosion depths at the lava source are ~0.6–0.8 m, a factor of ~3.6 lower than those pertaining to a similar scenario where presence of bubbles is not accommodated.

Could a 30 m thick flow that originally contains 30 vol % bubbles travel the 1400 km distance and still flow turbulently? First, it must be noted that bubbles are likely to decrease downstream of the source region and over time [*Swanson*, 1973]. Second, the Reynolds number characterizing this gas-enriched flow at the source region (~6.7×10^4) is higher by a factor of ~1.2 compared to the value (~5.6×10^4) referred to a flow of similar thickness, which is erupted at a temperature of 1250°C (Table 3), and is—on average—found to flow turbulently out to the total distance traveled by the Athabasca flood lava (Figure 6). Table 5 shows the changes in the Reynolds number and the initial bulk density and viscosity of the flow, which are associated with 30–65 vol % bubbles in the flowing lava. For 50 vol % bubbles, the Reynolds number of a 30 m thick flow at the source is equal to ~2.1×10^4, a factor of ~2.6 lower than 5.6×10^4. This flow would be characterized by a bulk density of 1410 kg/m^3 and an effective flow viscosity of 17.3 Pa s. For a lava flow containing 65 vol % bubbles, the flow regime always becomes laminar at a downstream distance that depends on the initial value of the lava flow thickness. At the source, the effective viscosity of the flow increases to 42.4 Pa s and the bulk density becomes as low as 988 kg/m^3.

In summary, our model results suggest that if the Athabasca lavas were enriched in gas (derived either from juvenile volatiles or from assimilation of water vapor from melting of substrate ice), then they would have been even less capable of thermal erosion to depths sufficient to produce the Athabasca channel. Lava-draped craters with depressed interiors (implying volume loss from closed depressions) suggest that a significant volume of gas was lost from the flow after eruption [*Jaeger et al*., 2010], so the lava was probably bubble rich near the vent.

4. Discussion

In this section, we discuss the possible sources of error for the model. Three values of eruption temperature (1270°C, the liquidus, and temperatures 10° and 20° below that) were chosen to investigate the extent to which this physical parameter may have affected other physical parameters of the flow and, ultimately, erosion rates and depths. As lava temperature reaches the value of 1243°C, the model stops producing turbulent flow. As a result, we do not expect the minimum eruption temperature to have been much lower than what we model, if turbulent flow conditions best represent the Athabasca flood lava [*Jaeger et al*., 2010], and a negligible source of error is expected to arise from this approximation.

The lava substrate underlying the Athabasca flow was assumed to be of the same composition as the lava. However, the substrate could have a lower melting temperature than the overlying lava. Notwithstanding, the presence of ice in substrate pore space and its level of consolidation appear to have a greater impact than a change in major oxide abundances on maximum erosion rates and depths, as shown in *Williams et al*. [1998, 2005]. The rootless cones that pepper the floor of Athabasca Valles [*Jaeger et al*., 2007] may indicate that a nonhomogeneous substrate existed at several locations along Athabasca Valles. Also, rootless cones could have been caused by atmospherically emplaced ground ice, because it would be difficult for lava erosion to reach deep ice layers [*Dundas and Keszthelyi*, 2013].

A potentially more important source of error in our model could result from our assumption of low strain rates in assessing the impact of bubbles on flow viscosity. Recent experimental and theoretical works explored the effects of bubbles on lava bulk viscosity under steady state flow [*Stein and Spera*, 2002; *Llewellin et al*., 2002; *Pal*, 2003; *Rust et al*., 2003]. *Llewellin et al*. [2002] developed a semiempirical constitutive model for the viscoelastic rheology of bubble suspensions with gas volume fractions <0.5 and small

deformations (capillary number = Ca ≪ 1). Their model was validated against observations of the deformation of suspensions of nitrogen bubbles in a Newtonian liquid (golden syrup) subjected to forced oscillations over a range of frequencies, *f*. In the case of steady-flow conditions, shear conditions remained constant for a time significantly longer than the relaxation time of the bubbles [*Llewellin et al*., 2002]. In a similar scenario, at low *f*, which occurs at low Ca values, bubbles remain approximately spherical in shape and increasing gas volume proportions, f_v, lead to an increase in bulk viscosity. At high *f*, which corresponds to high Ca values, bubbles are significantly elongate and viscosity decreases as the proportion of gas bubbles increases. Hence, viscosity can increase or decrease with increasing f_v depending on the conditions of strain. To date, the behavior of bubble-bearing turbulent lava has not been reproduced in any experimental setting. If we assumed that the viscosity of the bubble-rich flow became lower than that of the bubble-free flow by an order of magnitude, thus reaching a value of ~0.23 Pa s, the maximum erosion depths for 20 m thick lava flows—would be higher by a factor of ~2.3. Even if such a decrease in viscosity with increasing bubble contents were the case, other factors such as variations in effusion rates with time would likely act against a monotonic decrease. Other factors, such as local variations in slope, could also counteract such a trend of decrease in flow viscosity, especially along the steeper and more irregular portion of the proximal Athabasca channel.

Enhanced cooling caused by the effect of bubbles on thermophysical properties is not fully included in our analysis, though we do include the reduced lava density that represents the predominant effect of bubbles [*Keszthelyi*, 1994]. Consideration of these additional assumptions and conditions, while contributing to a more complete knowledge of the processes that may have occurred during the flow and emplacement of the Athabasca flood lava, is unlikely to lead to significantly higher erosion rates and erosion depths of the lava substrate.

Results show that the short flow duration poses a severe constraint on the ability of the lava to thermally erode the substrate. The maximum value of erosion depth obtained is far lower than the depth of the channel. Therefore, some additional mechanism besides thermal erosion must have been at work to erode Athabasca Valles. One possibility is that the channel was preexisting, produced either by aqueous floods [*Tanaka and Scott*, 1986; *Edgett and Rice*, 1995; *Burr et al*., 2002] or by a series of previous lava flows with modest erosional effectiveness [*Plescia*, 1990; *Keszthelyi et al*., 2004]. To better understand the latter possibility, mechanical erosion by lava must be examined in more detail. Mechanical erosion does not require long flow durations to generate high levels of erosion of the lava substrate. *Ciesla and Keszthelyi* [2000] suggested that many lava flows are close to reaching the critical stresses necessary to fracture underlying rock and entrain the fragments in the flow. They came to this conclusion by using a simple quantitative model of the stresses generated at the base of an active lava flow [*Hallet*, 1996]. In the model, lava is assumed to flow laminarly over a horizontal saw-toothed shaped substrate resulting in a cavity filled with a rotating pool of lava. *Ciesla and Keszthelyi* [2000] derived an expression from *Hallet* [1996], which enables determination of the average normal stress at the flow/substrate contact and, ultimately, calculation of the tensile stress in the rock. The latter was found to approximate or even reach the critical stresses required to fracture coherent crystalline rock. At Athabasca Valles, a similar scenario is supported by the presence of landforms that are consistent with (but not diagnostic of) mechanical erosion by lava, such as subrounded, lava-coated boulders several meters in diameter, which are often arranged in chains parallel to the flow direction [*Keszthelyi et al*., 2014]. At least some of these boulders may have been transported both on top of, and within, the lava flow, something that would be expected in a mechanically eroding lava flow. *Keszthelyi et al*. [2014] further suggest that the dune-like features that dot portions of the Athabasca channel floor may consist of a thin lava crust draped over hummocks of solid material that were transported within the flow and are thus potentially associated with mechanical erosion by lava. For the obtained short flow durations (Tables 3 and 5), the effect of mechanical erosion could be much stronger than thermal erosion because (1) larger entrained blocks do not reach thermal equilibrium with the flowing lava and (2) there may be a substantial porosity in the removed material [*Keszthelyi et al*., 2014]. Mechanical erosion physically removes portions of substrate that are not given sufficient time to become assimilated into the flowing lava. These entrained fragments and blocks could then contribute to eroding the substrate further by abrasion [*Ciesla and Keszthelyi*, 2000; *Siewert and Ferlito*, 2008]. *Keszthelyi et al*. [2014] place an upper limit on the amount of mechanical erosion obtainable at Athabasca Valles using thermal considerations. Specifically, rock is of the order 1000 K colder than the lava and the lava will freeze if cooled ~100 K, so the entrained rock should be no more than 10% of the erupted volume. Given the large distance traveled by the lava (~1400 km), an order of magnitude less

entrainment is likely more realistic. Using the available volume estimates of 5000 and 7500 km^3 [*Jaeger et al*., 2010], this corresponds to an order of ~100–1000 km^3 of erosion. Athabasca Valles is roughly 300 km × 30 km in area (~10,000 km^2), so a maximum of <100 m, and more realistically ~10 m average downcutting is allowed and nonuniform erosion—with some tens of meters of downcutting—could be reached locally. This is broadly consistent with results from Kasei Valles, where a similar turbulent lava flow is thought to have eroded large volumes at cataracts but had much lesser effects elsewhere [*Dundas and Keszthelyi*, 2014]. We will develop a new mechanical and thermomechanical model of erosion by turbulently flowing lava to test the validity of the predictions concerning the Athabasca flood lava.

5. Conclusions

The Athabasca Valles flood lava was probably emplaced turbulently, over a few to several weeks [*Jaeger et al*., 2010]. We apply the *Williams et al*. [2000a, 2005] model to investigate how effective the mechanism of thermal erosion by turbulent lava could have been in eroding the lava substrate along the ~75 km long upstream portion of the main Athabasca channel. Eruption temperatures within 20°C of the liquidus value (1270°C) were considered, and proportions of bubbles of 30%, 50%, and 65% by volume were assumed to coexist with the liquid phase within the flowing lava. For emplacement volumes of 5000 and 7500 km^3 and average lava flow thicknesses of 20 and 30 m, we find flow durations of ~11 to ~37 days, consistent with previous results from *Jaeger et al*. [2010]. The highest values of erosion depth are found at the lava source for a 20 m thick flow that is erupted at the liquidus temperature (1270°C) and flows free of bubbles over a substrate that contains 25% by volume of ice. The calculated erosion depths are never higher than 7.6 m, far less than the channel depth, indicating that thermal erosion played a negligible role in the formation of Athabasca Valles.

Notation

α	ground (substrate) slope, degree.
c_l	lava liquid-specific heat, J/kg °C.
c_g	substrate-specific heat, J/kg °C.
c_{vap}	water vapor-specific heat, J/kg °C.
c_w	substrate water/ice-specific heat, J/kg °C.
D	erosion depth into lava substrate, m.
E_{dg}	energy required to disaggregate substrate, J/m^3.
E_{hg}	energy required to heat the disaggregated substrate up to the lava temperature, J/m^3.
E_{mg}	energy required to melt substrate, J/m^3.
f_v	volume fraction of bubbles in lava.
f_w	volume fraction of water in substrate.
g	acceleration due to gravity, m/s^2.
h	lava flow thickness, m.
h_T	lava heat transfer coefficient, J/m s °C.
k_{eff}	lava effective thermal conductivity, J/m s °C.
k_g	substrate thermal conductivity, J/m s °C.
L_g	substrate heat of fusion, J/kg.
L_l	lava heat of fusion/crystallization, J/kg.
L_{vap}	heat of vaporization of water, J/kg.
μ_b	lava bulk viscosity, Pa s.
μ_{eff}	lava bulk viscosity (liquid, solid, gas), Pa s.
μ_g	substrate melt viscosity, Pa s.
μ_l	lava liquid viscosity, Pa s.
Pr	lava Prandtl number.
ρ_b	lava bulk density, kg/m^3.
ρ_g	substrate density, kg/m^3.
ρ_{gas}	water vapor density, kg/m^3.

ρ_l lava liquid density, kg/m^3.
ρ_w substrate water density, kg/m^3.
Q_0 initial flow rate, m^2/s.
$Q(x)$ initial flow rate, m^2/s.
Re lava Reynolds number.
r_h hydraulic radius, m.
$S(x)$ lava contamination.
t flow duration, days.
t_a flow duration, if total lava volume is 5000 km^3, days.
t_b flow duration, if total lava volume is 7500 km^3, days.
T lava temperature, °C.
T_a ambient temperature at martian surface, °C.
T_e eruption temperature at source vent, °C.
T_{liq} lava liquidus temperature, °C.
T_{mg} substrate melting temperature, °C.
T_{sol} lava solidus temperature, °C.
T_{vap} water vaporization temperature, °C.
u lava flow velocity, m/s.
u_m erosion rate of substrate, m/s.
V_{eff} total flow volume (liquid, solid, and gas), km^3.
x distance from source vent, m.
X volume fraction of crystals.
$X'(T)$ rate of change of olivine crystals fraction with temperature.

Acknowledgments

The investigation by Vincenzo Cataldo and David A. Williams was supported by NASA Planetary Geology and Geophysics grant NNX12AR66G. We used data obtained from the NASA Planetary Data System, and the Ronald Greeley Center for Planetary Studies (the NASA Regional Planetary Information Facility at ASU). We are grateful to all those who were involved in analyzing the data collected by the High Resolution Imaging Science Experiment (HiRISE), Context (CTX), and Compact Reconnaissance Imaging Spectrometer for Mars (CRISM) instruments onboard the Mars Reconnaissance Orbiter (MRO) spacecraft. Specifically, the data contained in the *Jaeger et al.* [2007, 2010] papers enabled production of our results. Finally, we are grateful for the constructive comments by journal reviewers, and Michael Bland and Christopher Edwards.

References

Arndt, N. T. (1976), Melting relations of ultramafic lavas (komatiites) at one atmosphere and high pressure, *Year Book Carnegie Inst. Washington*, *75*, 555–562.
Baird, A. K. (1984), Did komatiitic lavas erode channels on Mars?, *Nature*, *311*, 18.
Baker, V. R., G. Komatsu, T. J. Parker, V. C. Gulick, J. S. Kargel, and J. S. Lewis (1992), Channels and valley on Venus: Preliminary analysis of Magellan data, *J. Geophys. Res.*, *97*, 13,421–13,444, doi:10.1029/92JE00927.
Bandfield, J. L., V. E. Hamilton, and P. R. Christensen (2000), A global view of Martian surface compositions from MGS-TES, *Science*, *287*, 1626–1630.
Berman, D. C., and W. K. Hartmann (2002), Recent fluvial, volcanic, and tectonic activity on the Cerberus Plains of Mars, *Icarus*, *159*, 1–17.
Bird, R. B., W. E. Stewart, and E. N. Lightfoot (1960), *Transport Phenomena*, 780 pp., John Wiley, New York.
Bottinga, Y., and D. F. Weill (1970), Densities of liquid silicate systems calculated from partial molar volumes of oxide components, *Am. J. Sci.*, *269*, 169–182.
Burr, D. M., J. A. Grier, A. S. McEwen, and L. P. Keszthelyi (2002), Repeated aqueous flooding from the Cerberus Fossae: Evidence for very recently extant, deep groundwater on Mars, *Icarus*, *159*, 53–73.
Caricchi, L., L. Burlini, P. Ulmer, T. Gerya, M. Vassalli, and P. Papale (2007), Non-Newtonian rheology of crystal-bearing magmas and implication for magma ascent dynamics, *Earth Planet. Sci. Lett.*, *264*, 402–419.
Carr, M. H. (1974), The role of lava erosion in the formation of lunar rilles and Martian channels, *Icarus*, *22*, 1–23.
Champallier, R., M. Bystricky, and L. Arbaret (2008), Experimental investigation of magma rheology at 300 MPa: From pure hydrous melt to 76 vol.% of crystals, *Earth Planet. Sci. Lett.*, *267*, 571–583.
Chevrel, M. O., D. Baratoux, K. Hess, and D. B. Dingwell (2014), Viscous flow behavior of tholeiitic and alkaline Fe-rich Martian basalts, *Geoch. Cosmoch. Acta*, *124*, 348–365.
Christensen, P. R., R. V. Morris, M. D. Lane, J. L. Bandfield, and M. C. Malin (2001), Global mapping of Martian hematite mineral deposits: Remnants of water-driven processes on early Mars, *J. Geophys. Res.*, *106*(E10), 23,873–23,885, doi:10.1029/2000JE001415.
Ciesla, F. J., and L. Keszthelyi (2000), A simple model for lava flow quarrying: Mechanical erosion of the substrate *Proc. Lunar and Planet. Sci. Conf.*, *XXXI*, #1647.
Coombs, C. R., B. R. Hawke, and L. Wilson (1988), Geologic and remote sensing studies of Rima Mozart, *Proc. Lunar Planet. Sci. Conf. 18th*, 339–353.
Cutts, J. A., W. J. Roberts, and K. R. Blasius (1978), Martian channels formed by lava erosion (abstract), *Lunar and Planet. Sci. Conf.*, *IX*, 209.
Dundas, C., and L. P. Keszthelyi (2013), Modeling steam pressure under Martian lava flows, *Icarus*, *226*, 1058–1067.
Dundas, C., and L. P. Keszthelyi (2014), Emplacement and erosive effects of lava in south Kasei Valles, Mars, *J. Volcanol. Geotherm. Res.*, *282*, 92–102.
Edgett, K. S., and J. Rice (1995), Very young volcanic, lacustrine, and fluvial features of the Cerberus N Elysium basin region, Mars: Where to send the 1999 Mars surveyor lander (abstract), *Lunar Planet. Sci.*, *XXVI*, 357–358.
Gellert, R., et al. (2004), Chemistry of rocks and soils in Gusev crater from the Alpha Particle X-Ray Spectrometer, *Science*, *305*, 829–832.
Ghiorso, M. S., and R. O. Sack (1995), Chemical mass transfer in magmatic processes IV. A revised and internally consistent thermodynamic model for the interpolation and extrapolation of liquid–solid equilibria in magmatic systems at elevated temperatures and pressures, *Contrib. Mineral. Petrol.*, *119*, 197–212.
Greeley, R., S. A. Fagents, R. S. Harris, S. D. Kadel, D. A. Williams, and J. E. Guest (1998), Erosion by flowing lava: Field evidence, *J. Geophys. Res.*, *103*, 27,325–27,346, doi:10.1029/97JB03543.

Greeley, R., B. H. Foing, H. Y. McSween, G. Neukum, P. Pinet, M. Van Kan, S. C. Werner, D. A. Williams, and T. E. Zegers (2005), Fluid lava flows in Gusev crater, Mars, *J. Geophys. Res.*, *110*, E0500, doi:10.1029/2005JE02401.
Hallet, B. (1996), Glacial quarrying: A simple theoretical model, *Ann. Glaciol.*, *22*, 1–8.
Head, J. W., et al. (2011), Flood volcanism in the northern high latitudes of Mercury revealed by MESSENGER, *Science*, *333*, 1853–1856, doi:10.1126/science.1211997.
Hon, K., J. Kauahikaua, R. Denlinger, and K. Mackay (1994), Emplacement and inflation of pahoehoe sheet flows: Observations and measurements of active lava flows on Kilauea volcano, Hawaii, *Geol. Soc. Am. Bull.*, *106*, 351–370.
Hulme, G. (1973), Turbulent lava flows and the formation of lunar sinuous rilles, *Mod. Geol.*, *4*, 107–117.
Huppert, H. E., and R. S. J. Sparks (1985), Komatiites, I, eruption and flow, *J. Petrol.*, *26*, 694–725.
Huppert, H. E., R. S. J. Sparks, J. S. Turner, and N. T. Arndt (1984), Emplacement and cooling of komatiite lavas, *Nature*, *309*, 19–22.
Hurwitz, D. M., C. I. Fassett, J. W. Head, and L. Wilson (2010), Formation of an eroded lava channel within an Elysium Planitia impact crater: Distinguishing between a mechanical and thermal origin, *Icarus*, *210*, 626–634.
Jaeger, W. L., L. P. Keszthelyi, A. S. McEwen, C. M. Dundas, and P. S. Russell (2007), Athabasca Valles, Mars: A lava-draped channel system, *Science*, *317*, 1709–1711, doi:10.1126/science.1143315.
Jaeger, W. L., et al. (2010), Emplacement of the youngest flood lavas on Mars: A short, turbulent story, *Icarus*, *205*, 230–243.
Jarvis, R. A. (1995), On the cross-sectional geometry of thermal erosion channels formed by turbulent lava flows, *J. Geophys. Res.*, *100*, 10,127–10,140, doi:10.1029/95JB00027.
Keszthelyi, L. (1994), Calculated effect of vesicles on the thermal properties of cooling basaltic lava flows, *J. Volcanol. Geotherm. Res.*, *63*, 257–266.
Keszthelyi, L., T. Thordarson, A. McEwen, H. Haack, M. N. Guilbaud, S. Self, and M. J. Rossi (2004), Icelandic analogs to Martian flood lavas, *Geochem. Geophys. Geosyst.*, *5*, Q11014, doi:10.1029/2004GC000758.
Keszthelyi, L., S. Self, and T. Thordarson (2006), Flood lavas on Earth, Io, and Mars, *J. Geol. Soc. London*, *163*, 253–264.
Keszthelyi, L., W. Jaeger, C. M. Dundas, D. A. Williams, and V. Cataldo (2014), Evidence for possible mechanical erosion by lava at Athabasca Valles, Mars from HiRISE and CTX images and topography, *Lunar Planet. Sci.*, *45*, abstract 1683.
Lange, R. A., and A. Navrotsky (1992), Heat capacities of Fe_2O_3-bearing silicate liquids, *Contrib. Mineral. Petrol.*, *110*, 311–320.
Lejeune, A., and P. Richet (1995), Rheology of crystal-bearing silicate melts: An experimental study at high viscosities, *J. Geophys. Res.*, *100*, 4215–4229, doi:10.1029/94JB02985.
Leverington, D. W. (2011), A volcanic origin for the outflow channels of Mars: Key evidence and major implications, *Geomorphology*, *132*, 51–75.
Llewellin, E. W., H. M. Mader, and S. D. R. Wilson (2002), The rheology of a bubbly liquid, *Proc. R. Soc. A*, *458*(2020), 987–1016, doi:10.1098/rspa.2001.0924.
Malin, M. C., et al. (2007), Context camera investigation on board the Mars Reconnaissance Orbiter, *J. Geophys. Res.*, *112*, E05S04, doi:10.1029/2006JE002808.
McEwen, A. S., et al. (2007), Mars Reconnaissance Orbiter's High Resolution Imaging Science Experiment (HiRISE), *J. Geophys. Res.*, *112*, E05S02, doi:10.1029/2005JE002605.
McEwen, A. S., L. P. Keszthelyi, and J. A. Grant (2012), Have there been large recent (Mid-Late Amazonian) water floods on Mars?, *Lunar and Planet. Sci.*, *43*, abstract 1612.
McSween, H. Y., et al. (2004), Basaltic rocks analyzed by the Spirit rover in Gusev crater, *Science*, *305*, 842–845.
McSween, H. Y., et al. (2008), Mineralogy of volcanic rocks in Gusev crater, Mars: Reconciling Mossbauer, Alpha Particle X-Ray Spectrometer, and Miniature Thermal Emission Spectrometer spectra, *J. Geophys. Res.*, *113*, E06S04, doi:10.1029/2007JE002970.
Mo, X., I. S. E. Carmichael, M. Rivers, and J. Stebbins (1982), The partial molar volume of Fe_2O_3 in multicomponent silicate liquids and the pressure dependence of oxygen fugacity in magmas, *Mineral. Mag.*, *45*, 237–245.
Morris, R. V., et al. (2008), Iron mineralogy and aqueous alteration from Husband Hill through Home Plate at Gusev Crater, Mars: Results from the Mössbauer instrument on the Spirit Mars Exploration Rover, *J. Geophys. Res.*, *113*, E12S42, doi:10.1029/2008JE003201.
Murchie, S., et al. (2007), Compact Reconnaissance Imaging Spectrometer for Mars (CRISM) on Mars Reconnaissance Orbiter (MRO), *J. Geophys. Res.*, *112*, E05S03, doi:10.1029/2006JE002682.
Navrotsky, A. (1995), Energetics of silicate melts, in *Structure, Dynamics and Properties of Silicate Melts*, *Rev. Mineralog. Geochem.*, vol. 32, edited by J. F. Stebbins, P. F. McMillan, and D. B. Dingwell, pp. 121–144, Mineralog. Soc. of Am., Chantilly, Va.
Pal, R. (2003), Rheological behavior of bubble-bearing magmas, *Earth Planet. Sci. Lett.*, *207*, 165–179.
Pinkerton, H., and R. J. Stevenson (1992), Methods of determining the rheological properties of magma at sub-liquidus temperatures, *J. Volcanol. Geotherm. Res.*, *53*, 47–66.
Plescia, J. B. (1990), Recent flood lavas in the Elysium region of Mars, *Icarus*, *88*, 465–490.
Rust, A. C., M. Manga, and K. V. Cashman (2003), Determining flow type, shear rate and shear stress in magmas from bubble shapes and orientations, *J. Volcanol. Geotherm. Res.*, *122*, 111–132.
Schenk, P. M., and D. A. Williams (2004), A potential thermal erosion lava channel on Io, *Geophys. Res. Lett.*, *31*, L23702, doi:10.1029/2004GL021378.
Self, S., L. P. Keszthelyi, and T. Thordarson (1998), The importance of pahoehoe, *Annu. Rev. Earth Planet. Sci.*, *26*, 81–110.
Serway, R. A., and J. W. Jewett (2014), *Physics for Scientists and Engineers with Modern Physics*, 9th ed., 1622 pp., Brooks/Cole, Boston, Mass.
Shaw, H. R. (1972), Viscosities of magmatic silicate liquids: An empirical method of prediction, *Am. J. Sci.*, *272*, 870–893.
Shaw, H. R., and D. A. Swanson (1970), Eruption and flow rates of flood basalts, in *Proc. 2nd Columbia River Basalt Symposium*, edited by E. H. Gilmore and D. F. Stradling, pp. 271–299, East. Wash. State Coll. Press, Cheney.
Sibree, J. O. (1934), The viscosity of froth, *Trans. Faraday Soc.*, 325–331.
Siewert, J., and C. Ferlito (2008), Mechanical erosion by flowing lava, *Contemp. Phys.*, *49*(1), 43–54.
Spera, F. J., A. Borgia, J. Strimple, and M. Feigenson (1988), Rheology of melts and magmatic suspensions. 1. Design and calibration of concentric cylinder viscometer with application to rhyolitic magma, *J. Geophys. Res.*, *93*(B9), 10,273–10,294.
Stein, D. J., and F. J. Spera (2002), Shear viscosity of rhyolite-vapor emulsions at magmatic temperatures by concentric cylinder rheometry, *J. Volcanol. Geotherm. Res.*, *113*, 243–258.
Stolper, E., and H. Y. McSween (1979), Petrology and origin of the shergottite meteorites, *Geoch. Cosm. Acta*, *43*, 1475–1498.
Swanson, D. A. (1973), Pahoehoe flows from the 1969–1971 Mauna Ulu eruption, Kilauea volcano, Hawaii, *Geol. Soc. Am. Bull.*, *84*, 615–626.
Tanaka, K. L., and D. H. Scott (1986), The youngest channel system on Mars (abstract) *Lunar Planet. Sci.*, *XVII*, 865–866.
Treiman, A. H. (2005), The nakhlite meteorites: Augite-rich igneous rocks from Mars, *Chemie der Erde-Geoch.*, *65*, 203–270.
Usselman, T. M., D. S. Hodge, A. J. Naldrett, and I. H. Campbell (1979), Physical constraints on the characteristics of nickel-sulfide ore in ultramafic lavas, *Can. Mineral.*, *17*, 361–372.

Wadge, G. (1981), The variation of magma discharge during basaltic eruptions, *J. Volcanol. Geotherm. Res.*, *11*, 139–168.
Williams, D. A., R. C. Kerr, and C. M. Lesher (1998), Emplacement and erosion by Archean komatiite lava flows at Kambalda: Revisited, *J. Geophys. Res.*, *103*, 27,533–27,549, doi:10.1029/97JB03538.
Williams, D. A., S. A. Fagents, and R. Greeley (2000a), A reassessment of the emplacement and erosional potential of turbulent, low-viscosity lavas on the Moon, *J. Geophys. Res.*, *105*(E8), 20,189–20,205, doi:10.1029/1999JE001220.
Williams, D. A., A. H. Wilson, and R. Greeley (2000b), A komatiite analog to potential ultramafic materials on Io, *J. Geophys. Res.*, *105*, 1671–1684, doi:10.1029/1999JE001157.
Williams, D. A., R. Greeley, E. Hauber, K. Gwinner, and G. Neukum (2005), Erosion by flowing Martian lava: New insights for Hecates Tholus from *Mars Express* and *MER* data, *J. Geophys. Res.*, *110*, E05006, doi:10.1029/2004JE002377.
Williams-Jones, G., A. Williams-Jones, and J. Stix (1998), The nature and origin of Venusian canali, *J. Geophys. Res.*, *103*(E4), 8545–8555, doi:10.1029/98JE00243.
Wilson, L., and P. J. Mouginis-Mark (1984), Martian sinuous rilles (abstract) *Lunar and Planet. Sci.*, *XV*, 926–927.
Wilson, L., and P. J. Mouginis-Mark (2001), Estimation of volcanic eruptions conditions for a large flank event on Elysium Mons, Mars, *J. Geophys. Res.*, *106*, 20,621–20,628, doi:10.1029/2000JE001420.
Zuber, M. T., D. E. Smith, S. C. Solomon, D. O. Muhleman, J. W. Head, J. B. Garvin, J. B. Abshire, and J. L. Bufton (1992), The Mars Observer Laser Altimeter investigation, *J. Geophys. Res.*, *97*, 7781–7797, doi:10.1029/92JE00341.